https://doi.org/10.56801/MME907

Numerical and experimental investigations of mechanical properties of AW 6005-T6 Aluminium alloy butt weld joint using GMAW process

Benoit Ndiwe[1,2,3], Paul Kah[1], Francois NjockBayock[3], Daniel AgiliUchechukwu[1], Harrison Onyeji[1]

[1]Department of Engineering Science, University West, 46186 Trollhättan, Sweden
[2]Laboratory of Welding Technology, Lappeenranta University of Technology, P.O. Box 20, 53851 Lappeenranta, Finland
[3]Department of Mechanical Engineering, ENSET Douala, University of Douala, PO Box: 1872, Douala, Cameroon

Received: 08-10-2022
Accepted: 31-03-2023

Abstract:This study aimed to investigate the effect of the welding heat input on the heat affected zone (HAZ) of AW 6005-T6 aluminium alloy for a butt-welded joint using gas metal arc welding (GMAW). The study involved using a welding experiment, numerical simulation, physical simulation, and mechanical tests. The welding was carried out using the pulsed GMAW transfer, and type J thermocouples were used to develop the thermal cycles in the HAZ. Simufact® Welding was utilized for the numerical simulation. An optical microscope was used to evaluate the microstructures and the Vickers microhardness test was done along the weld cross-section. The HAZ was located on the weld cross-section with a mean hardness of 63.7 HV, which is considerably lower when compared with the base metal (BM) which has a hardness of 100 HV. This indicates thermal softening occurred due to the heat input to the material. There is a match in the hardness values of the Gleeble samples and the locations on the weld cross section suggested by the model showing the validity of the simulation. It is important to note the fact that there is an influence of heat input into aluminum AW 6005-T6 weld joints and its mechanical properties in the design of welding process parameters for automotive parts. The welding parameters can be optimized to decrease the heat input into the weld, as this can directly affect the mechanical properties in the HAZ.

Keywords:W 6005-T6, HAZ, Simufact Welding, thermal cycle, Gleeble peak temperatures, Vickers hardness

1. Introduction

The increase in the demand to produce vehicles with light weight to promote better fuel consumption efficiency and less CO_2 emission has led to the study of aluminium alloys as a material for the construction of automobile parts such as the battery tray of electric vehicles[1; 2]. In recent years, the aluminium alloy-based components in an automobile have doubled because of their favorable properties of light weight, sufficient strength, corrosion resistance, recyclability, and good formability of parts. Its high thermal conductivity, high

*Corresponding authors: Benoit Ndiwe, benoit.ndiwe@student.lut.fi

thermal expansion property, averaging for precipitation-hardening alloys, and susceptibility to form aluminium oxides thereby having a higher melting point present difficulties in welding the alloy [1-4].

Heat-treatable aluminium, alloyed with Mg, and Si are widely used in the engineering industry today because of its favorable mechanical properties and weldability [2; 4]. An example of the such alloy is the AW 6005-T6 alloy which is used in the construction, automobile industry, shipbuilding, pipelines, railway, and furniture tubing [5]. It lies in the 6xxx class of extruded aluminium alloys. According to litterature, this class of aluminum alloy is known for its good malleability, excellent ductility, high corrosion resistance in marine applications, low density, excellent thermal conductivity and excellent weldability [6-8].

Siwowski et. al. researched AW6005 and found out that the HAZ in a welded structure is the point for potential failure in the weld when subjected to load [9]. As a result, it is important to determine the heat and stress distribution in the HAZ of the welded aluminium joints [10]. The distribution of heat and stress in the aluminium alloy depends on; the thickness of the plate being joined, the amount of heat input', the joint type, the number of weld passes, the shielding gas, and the clamping system. Considering all these factors and their possible interactions with each other, it is extremely complicated to track. Several pre-production welding trials may be required, and this becomes expensive. Simulation involves computing the approximate behavior of an operation over a period of time. This promotes the application of finite element (FE) based numerical simulation of the welding process to achieve accurate prediction of the thermal cycles, distortion, and residual stress in the operation. FE simulation takes advantage of a proven mathematical model from Goldak double ellipsoidal heat source [11] to approximate what happens in the welding process [12].

The thermal cycle simulation of the HAZ in welded joints is useful in determining the product quality of the weld. It can be followed by investigations of mechanical properties [13]. The HAZ which will encounter different thermal cycles will have a change in its properties depending on the strengthening mechanism of the aluminium alloy. These in-situ changes in the properties can then be investigated with the knowledge of the heat treatment of the HAZ using numerical simulation of the HAZ in welded joints [14].

A major problem with fusion welding as stated earlier is the thermal cycles which affect the microstructure and therefore the mechanical properties in weld joints [10; 15]. The thermal cycle effects depend on the heat input to the alloy which brings about the thermal softening of the aluminium alloy [16]. A less expensive approach for research to investigate the thermal cycles is by numerical simulation method. This aids in reducing the number of required experiments in the research and development of material.

Regarding the stated problems the following questions have been developed for this research; does the numerical simulation of the HAZ complement the investigation of welding experiment with thermocouples? Can a developed numerical model for a welding condition be used to predict the thermal cycles for other welding operations with varying parameters? What is the effect of the heat input on the mechanical property of the HAZ for AW 6005-T6 due to GMAW?

The objectives of this research are as follows; i) to develop FE model representing the welding condition in the joint from predefined welding parameters, ii) to ascertain the thermal cycle at several points in the HAZ of the AW 6005-T6 alloy using numerical simulation software, Simufact Welding®, iii) to examine the microstructures of the HAZ in the welded joint, iv) to obtain the microhardness property of the HAZ in the weld cross-section.

The peak temperature of the aluminium alloy at different points in the HAZ is a function of the distance from the weld zone, also the temperature and time tell the heat treatment experienced by the alloy. This determines the microstructure that will exist at the location and hence the mechanical properties of the alloy in the zone.

The findings gotten from the research aims above will be used to design a welding process to manufacture a crashworthy aluminium battery tray for Volvo electric cars. The analysis of this research work is limited to the thermal effects (thermal model) on the mechanical properties of the HAZ in the alloy.

In numerical simulation research works, it is best to first carry out an actual experiment. This will give an idea of the process parameters and aid in calibrating the numerical simulation and mathematical models to be implemented that demonstrates the physical phenomenon occurring in the experimental process [17; 18].

Previous research [19] have explored and investigated the effect of the complex interaction of surface roughness, the residual stresses induced, the stability of the compressive residual stresses during fatigue cycles, and the work hardening of the surface layers induced by the shot peening process on the fatigue behavior of AA 6005-T6 aluminum alloy at room temperature. This work has investigated the HAZ of AW 6005-T6 butt welded using MIG pulse, numerical simulation was used to further complement the welding experiment results.

2. Materials and Methods

2.1. Base metal

The base metal (BM) utilized for this research is the AW 6005-T6 aluminium alloy with dimensions of 500 mm x 200 mm x 3 mm. The chemical elements composed of the alloy and their physical properties can be seen in table 1. The aluminium plates are placed in a butt joint configuration with predefined weld parameters and are to be welded along the length of the plate.

Table 1. *Chemical composition of AW 6005-T6 alloy in m% with Al composition balanced [15].*

	Si	**Fe**	**Cu**	**Mn**	**Mg**	**Zn**	**Ti**	**Cr**	**Mn + Cr**
Min	0.5	0.0	0.0	0.0	0.4	0.0	0.0	0.0	0.12
Max	0.9	0.35	0.3	0.5	0.7	0.2	0.1	0.3	0.5

Physical properties of AW 6005 alloy [20].

Density Kg/m³	Melting point°C	Latent Heat of MeltingJ/Kg	Thermal expansion1/K	UTS (MPa)
2.7	605-655	410000	24E-6	270

2.2. Equipments

2.2.1. Welding Setup

The welding operation was carried out with a 6 axes industrial robot, IRB 1400 at the Production Technology Centre (PTC), University West, to prevent the human variability factor for the research. The 6th axis of the robot arm is replaced with the GMAW torch, 5000 power source is used with ELGA Alumig AlSi5 (Al 4043A) as the feeder wire [21]. New welding parameters as seen in table 2 were adopted and used in the welding experiment.

Table 2. *Welding parameters*

Welding parameters	Value	Unit
Wire Diameter	1.2	mm
Current	121	A
Voltage	19.4	V
Weld Speed	10	mm/s
Wire Speed	5.3	m/min
Wire Stick Out	16	mm
Heat Input	0.188	KJ/mm

2.2.2. Weld experimental

The test sample was welded to set the parameters of the physical simulation. Real courses of the temperature cycle were obtained from welding. The joint was designed as a butt weld with a square groove on 3 mm thick AW 6005-T6 Al plates measured 500 mm by 200 mm in area. Welding was done by a linear robotized pulsed MIG welding machine, Fronius Trans-Pulse Synergic (TPS) 5000 CMT. The welding parameters that gave good surface quality in the weld trials were used as starting parameters in this experiment. The welding parameters were monitored with Fronius Explorer software. The following welding parameters were set in the welding machine for the weld. current = 120 A, wire feed speed = 5.3 m/min, voltage = 19.25 V, welding speed = 10mm/s, Stick out = 16 mm, Welding wire = ELGA Alumig Si5 (EN ISO 18273:S Al 4043A (AlSi5), wire diameter = 1.2 mm, shielding gas = 100% Argon (Ar). These welding parameters are also shown in Table 2.

A total of two joints were produced, one with ceramic backing and the other without ceramic. During the welding process, temperature cycles (heating and cooling) in the HAZ were recorded with the aid of TC using the LabVIEW software. J-type TC were tack-welded on the plate as shown in Figure 1. TC6 was harpooned into the weld pool during welding, hence it recorded the highest peak temperature value of 669.38°C in the cycle. The thermal cycle as recorded from this pre-test is shown in Figure 2, showing only the reading of the survived TC. The thermal cycle generated from the weld pre-test was used as input in the gleeble for physical simulation.

During the welding experiment thermocouple TC1, TC2 and TC5 burnt. Thermocouples TC3, TC4 and TC6 survived, and their thermal cycle was used as a base for the gleeble simulation input. The sketch of the welded plate showing the TC location is shown in Figure 1.b.

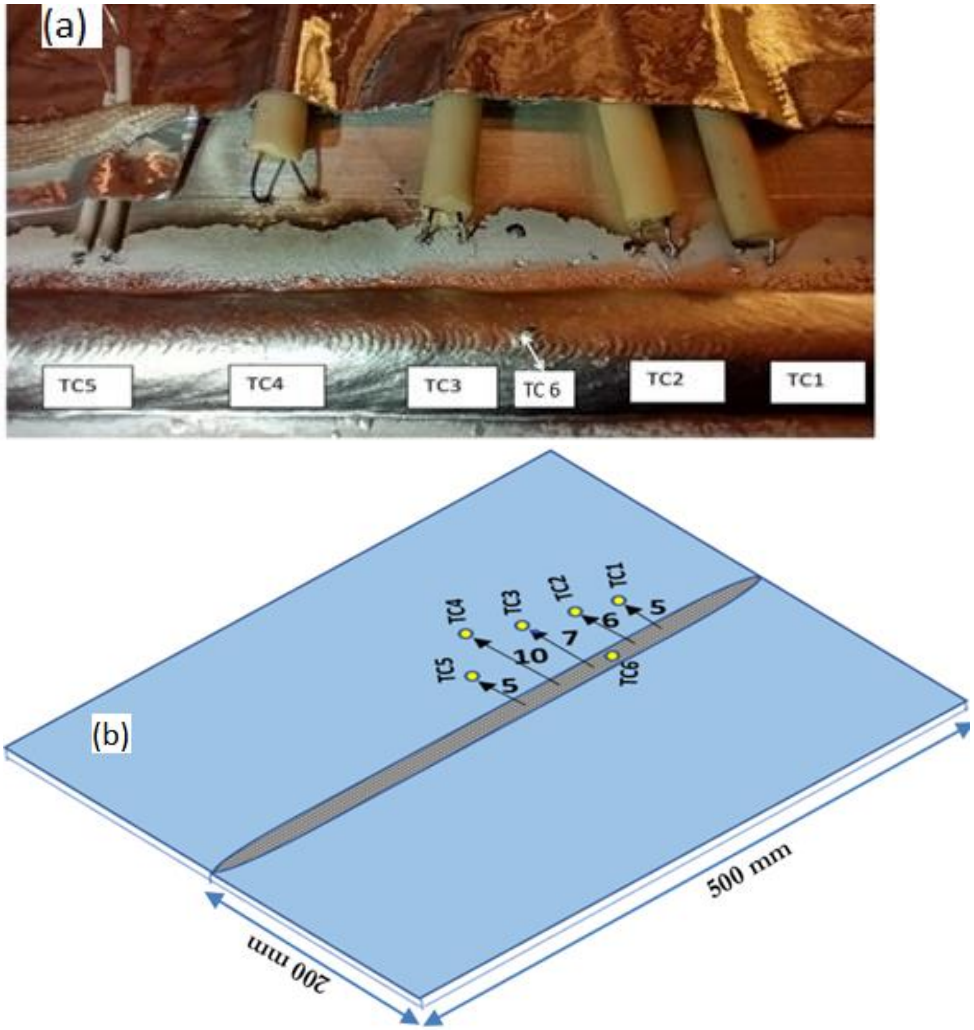

Figure 1. *a-Attached TC on the plate; b-Skitch of the welded plate with TC locations.*

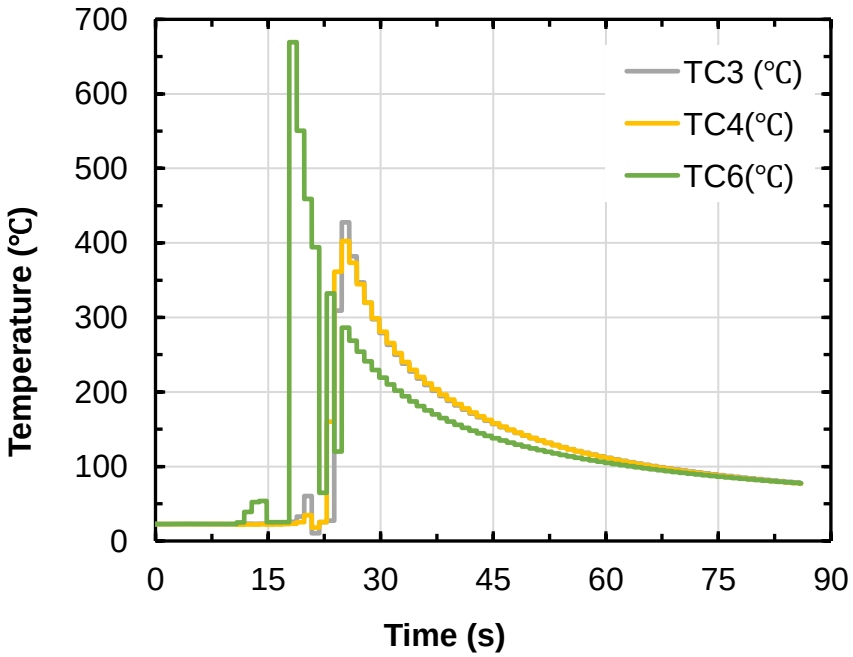

Figure 2. *Weld thermal cycles.*

2.2.3. Type J thermocouple

The type J thermocouple with its temperature sensitivity range between -210 and 750 ^{o}C, was used to measure the temperatures of aluminum alloy. It is made with a positive Iron (Fe) leg and a negative Copper-Nickel (Constantan) leg [22]. The materials used for the legs have good temperature sensitivity, the diameter of the thermocouple legs in this setup is 0.25 mm. The small cross-section of the thermocouple legs means the mass of the thermocouple is less, therefore the energy required by the thermocouple to make a measurement is minimized and the readings gotten are more accurate and can have a faster response time [23].

The thermocouple legs are joined to the aluminium plates by a discharge thermocouple welding machine and connected to the computer to record and output the temperature readings. The temperatures are recorded at a frequency of 75 Hz. Also, the thermocouple legs are insulated with foil so the heat content in the legs is not affected by the environmental conditions.

Six thermocouples are attached to the BM varying distances from the weld center line of the butt joint configuration. Table 3 shows the different thermocouple positions and figure 1 shows the experimental placement of the thermocouples.

Table 3. *Thermocouple positions for experiment*

Thermocouples	Distance from WCL (mm)	Distance from fusion boundary (mm)
TC 1	5	1
TC 2	6	2
TC 3	7	3
TC 4	10	6
TC 5	5	1
TC 6	2	Fusion zone

2.3. Numerical Simulation

2.3.1. Heat input model

The heat input model used for GMAW is Goldak's double ellipsoidal heat source model which was derived from the earlier ellipsoidal power density distribution model [11]. Goldak's model proposes to superimpose 2 ellipsoids, so an asymmetric heat input to the plate is simulated, the front half of the arc is a quadrant of the first ellipsoid and the rear half is another quadrant of the other ellipsoid. From the welding parameters of the heat source, V, I, the efficiency (η) of the power source, and the quantity of heat input to the plate (Q) can be gotten equation (Eq.1).

$$Q = \frac{V * I * \eta}{S} \tag{1}$$

Where:

V = voltage (volts), I = current (amperes), η = arc efficiency, S = welding speed (mm/s)

The intensity of the heat source follows a Gaussian distribution across the arc, which is noted as the heat flux (q), it is related to a, b, d (semi-axes of the ellipsoid along the x, y and z axes), τ (lag factor at a time "t" in the weld), Ff (Fraction of heat deposited in the front quadrant), Fr (Fraction of heat deposited in the rear quadrant) and is represented in the mathematical models for the fraction of heat deposited in the frontal and rear part of the arc respectively as shown in equations (Eq. 2) and (Eq. 3).

$$qf(x,\ y,\ z,\ t) = \frac{6*\sqrt{3}*Ff*Q}{a_f bd\pi\sqrt{\pi}} * e^{\frac{-3x^2}{af^2}} e^{\frac{-3y^2}{b^2}} e^{\frac{-3[z+v(\tau-t)^2]}{d^2}} \quad (2)$$

$$qr(x,\ y,\ z,\ t) = \frac{6*\sqrt{3}*Fr*Q}{a_r bd\pi\sqrt{\pi}} * e^{\frac{-3x^2}{ar^2}} e^{\frac{-3y^2}{b^2}} e^{\frac{-3[z+v(\tau-t)^2]}{d^2}} \quad (3)$$

$$Ff = \frac{2}{\left(1+\left(\frac{ar}{af}\right)\right)} \quad (4)$$

$$Fr = \frac{2}{\left(1+\left(\frac{af}{ar}\right)\right)} \quad (5)$$

$$Fr + Ff = 2 \quad (6)$$

2.3.2. Heat transfer model

Heat transfer is by contact, convection, conduction, and radiation and thus the amount of heat transferred is shown by the Qcht, Qcv, and Qr for equations (Eq.7, 8, and 9), while equation (Eq. 10) expresses how heat is transferred in an alloy by conduction [11].

$$Qcv = -hA\ (T_1 - T_2) \quad (7)$$

$$Qr = -\varepsilon A(T_1^4 - T_2^4) \quad (8)$$

$$Qcht\ =\ \alpha A(T_1 - T_2) \quad (9)$$

$$\frac{\Delta Q}{\Delta t} = KA\frac{\Delta T}{L} \quad (10)$$

Where:

h = convective transfer coefficient, α = contact heat transfer coefficient, ε= emission coefficient, A = surface area, T1 = Initial temperature, T2 = Final temperature, L = length of alloy, K = thermal conductivity of alloy.

2.3.3. Simulation

Simufact Welding® Finite Element Analysis software was used to solve the numerical model. The bead size specification from the welding experiment was measured and a Computer-Aided Design (CAD) model was created, meshed, and imported into the model. The weld bead from the experiment has an approximate height of 2.4 mm and a width of 8 mm. A 2-D plane strain FE model is built and the FE meshing is shown in Fig. 3. In total, 2144 nodes and 2022 elements are meshed, and imported into the model.

The clamps used are insulated with aluminium foil so that the heat loss through the clamps is prevented. There were also ceramic backings placed to support the weld joint underneath. An approximation to this is represented in the model by setting the clamp and backings to have zero (0 W/(m^2*k)) contact and convective heat transfer coefficients from equations 8 and 9. The boundary condition for the initial temperature is set to 23 ^{o}C for all the components in the model.

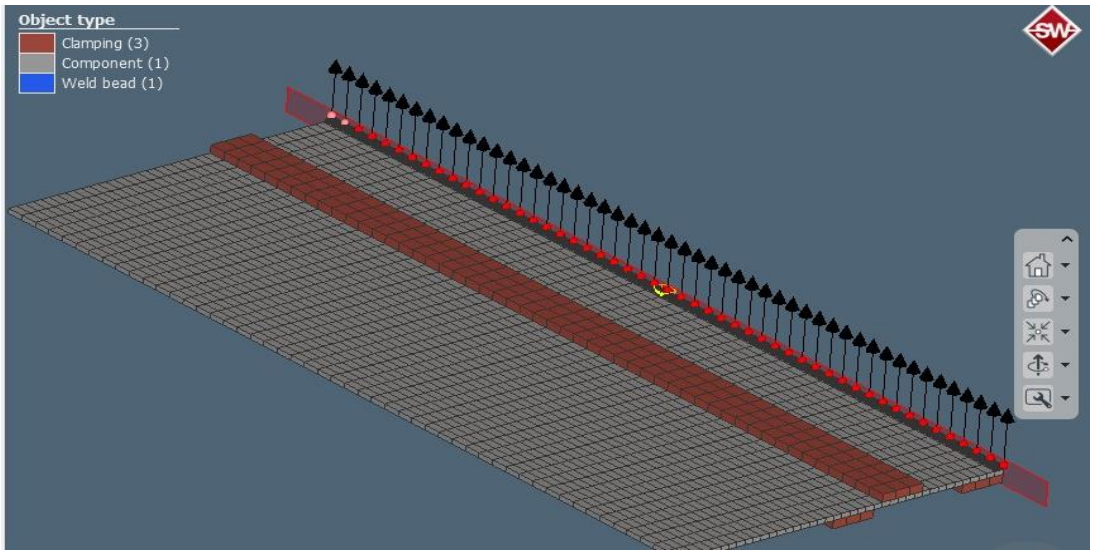

Figure 3. *Assembled model of welding setup with a symmetry plane.*

A symmetry plane is used, this reduces the number of elements and nodes thereby reducing the computation time. Hence, just one plate and half the bead are created for the CAD model. The components of the plate, bead, and clamps are imported into the model and assembled as seen in the setup. Welding parameters from table 2 are inputted into the model, and particles are added in positions the thermocouples were placed from table 4 to get the thermal cycles.

The heat source is applied at the top end of the weld bead and the welding direction is shown by the red dots. To ensure the accuracy of FE analysis, all the elements in the areas of computation have to be of smaller uniform size, the mesh refinement tool is used on the criterion of temperature gradient for the components.

Adaptive remeshing was used to refine the meshed elements of the model. The mesh is refined for each element in refinement levels. For each level, the size of an element is reduced by half. In this model, the mesh refinement is done with the criteria of a temperature gradient. The extent of the temperature gradient in the element determines if it would be refined. The temperature gradient factor to trigger the mesh refinement is set at 0.02.

The plate component is set to a refinement level of 3 while the bead refinement level is 1. The resulting minimum element size after refinement became 1 mm. As a result, there are more elements and nodes around the heat source where there is a temperature gradient in the model.

The BM properties for AW 6005-T6 are created in the Simufact Material module of the Simufact welding FE tool and imported into the model. The thermophysical values for specific heat capacity and thermal conductivity were imported and other constant value thermal properties for the materials from literature reviews are shown in Table 4 [15]. Likewise, for the filler wire material, the AlSi12_sw material is imported to the robot object in the Finite Element Model process tree. The filler material imported to Simufact welding model from the Simufact materials database is of the Al 4047 class and the thermal properties are given in Table 4.

The welding was carried out along the 500 mm length of the plate at the travel speed of 10 mm/s. This made the weld time 50 seconds. The cooling time is set at 15 seconds; therefore, the total analysis time is 65 seconds. The maximum change in temperature in each node per increment is set to 100 °C to control the time step length. A fixed time step of 0.05 seconds is used for each increment of the welding. The maximum error allowed between the estimated and solution temperature for each iteration was set to 20 °C and the relative residual tolerance for the model is set to 0.01. The maximum number of recycles per increment is 50,

and using a positive value tells Simufact to stop the simulation if no convergence is achieved in the simulation.

Various values for the Goldak heat source parameters are entered into the model to ensure the thermal cycle result matches the thermal cycle from the welding experiment. The welding parameter values are kept the same as in the welding experiment to get a valid model. The completed FE model before element refinement had 14944 nodes and 8950 elements, smaller than usual due to the use of a symmetry plane.

Table 4. *Thermal properties of welding filler material*

Properties	Value	Requirement	Units
Melting temperature	570 – 590	≤ 655	°C
Latent heat of fusion	390,000	≤410 000	J/Kg
Density	2.7		Kg/m³

2.4. Metallography

A Gleeble thermal simulation was carried out on the alloy with the pre-selected peak temperatures of 350, 450, and 550 °C, using the derived thermal cycle to get a larger representation of the HAZ. The Gleeble samples were water cut, so their microstructures can be observed in the optical microscope. Afterwards, the samples were cold mounted as shown in Figure 4.

The cold mounting process is done at room temperature in the cold mounting apparatus. The cold mounting material is then poured into the mould where the sample is placed and left.

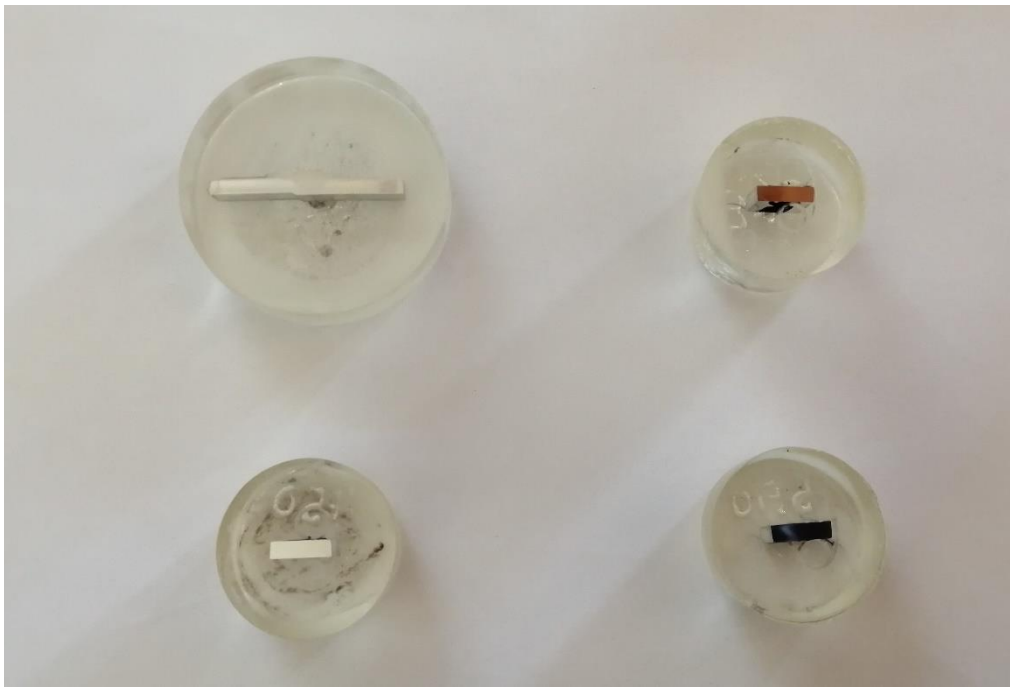

Figure 4. *Cold-mounted metallography samples.*

Each specimen is hand-grinded on the Buehler metaserv™ 250 with Buehler's P 1200, P 2500, and P 4000 Grit 1000 CarbimetSiC (Silicon carbide) using grinding paper at 200 rpm for a few seconds to get rid of the oxides on the sample. The samples are mounted for polishing on the Buehler Automet™ 300. The timer is set for 10 minutes with Mastermet 2 polishing fluid at 25 - 35 N force, on the Mastermet® aluminium polishing disc. In the last 2 minutes of the polishing, hydrogen peroxide is added to the polishing liquid to aid better

exposure of the grains in the microscope. The samples are washed in water and further cleaned with ethanol in the ultrasonic cleanser to get rid of fine particles of the polished alloys.

The etchant used is 1.8 % concentrated Barker's reagent. It is an electrolytic etchant, so the specimen is anodized at 20 V and the etchant is swapped over the specimen for 3-5 minutes till a reaction in the form of bubbles at the surface is seen [24]. The specimen is dried and ready for observation in the Zeiss Axioscope optical microscope with polarized light.

2.5. Gleeble experiments

The aluminium sheet which is used for this thermomechanical testing using Gleeble 3800 simulator is dog bone shape samples. The BM was supplied by Volvo cars and was cut using a water jet to the desired geometry/dimension as shown in Figure 5 from the supplied sheet in a T6 (solution heat treated and artificially aged) condition. Precise preparation of HAZ specimens with the required geometrical shape and good surface quality is indispensable for a successful simulation.

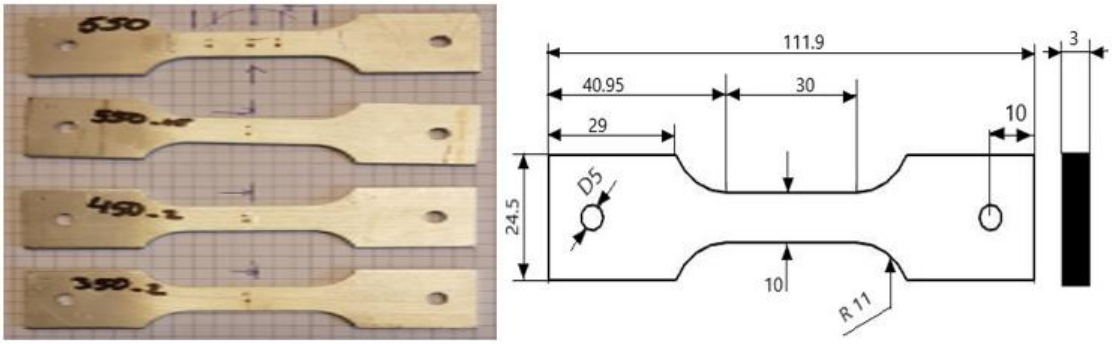

Figure 5. *Specimen geometry and dimension.*

2.6. Tensile test

The tensile test was performed using Gleeble 3800 according to EN ISO 6892-1:2016 [25]. The gleeble machine was set to unitension mode (uni-directional tension), this mode will activate the gleeble ram to move only in one direction as required for this experiment. The sample geometries/dimension are shown in Figure 4. The three specimen materials were heated to 350 ◦C, 450 ◦C, and 550 ◦C peak temperatures during the gleeble heat treatment. These specimens were cooled to room temperature in the air. At room temperature, these spacemen were subjected to a tensile test till fracture, and their response and behavior during the test were recorded with Labview software. These test for each specimen was repeated to validate the accuracy of the test.

2.7. Hardness test

Mechanical tests to determine the alloy's resistance to localised plastic deformation were carried out in a Vickers hardness tester. The microhardness of specimens 1, 2, 3 and 4 was carried out using the Struers™ hardness tester at different points on the specimens. The Vickers hardness was carried out with a load of 100g (HV) on the alloy and a dwell time of 12 seconds at a distance of 0.5 mm between each successive indentation according to EN ISO 9015-2 and EN ISO 6057-1 [26], for the linear hardness inquiry for the specimen 1. For specimens 2, 3 and 4 indentations were taken at different points on the sample taken at random.

3. Results

3.1. Welding experiments

Using the welding parameters of MIG pulse on joint 1 and joint 2, good quality welds were obtained without any spatter on the alloy surface. Upon visual inspection, it was seen to be a good fusion weld. The heat input for the new welding parameters computed from equation 1 is given to be 187.80 J/mm. The type J thermocouples 1, 2, and 5 close to the weld center line (WCL) were burnt off by the arc as seen in Figure 1. a. Thus, the thermal cycles from these positions were not retrievable from these points, the peak temperatures of the thermal cycles of the observed thermocouples 3, 4 and 6 are 427 ºC, 402 oC, and 669 ºC respectively.

It was observed on the thermal cycle that the cooling end of the curve for thermocouple 6 has a dip to 65 °C and rises again to 330 °C. This may be because thermocouple 6 is placed in the molten weld pool and as it is solidifying, this partially disrupts the thermocouple readings. Due to the heat from the arc, there is quick and constant heating on the plate. The cooling curves for the 3 thermocouples all follow a similar cooling trend regardless of their peak temperatures.

3.2. Numerical Simulation results

Various values for the Goldak double ellipsoidal heat source and film coefficient parameters were systematically entered into the simulation model to get a good match to the experimental thermal cycle. Figure 6 shows the thermal cycles for all thermocouples in the experiment gotten with parameters from Table 5.

Table 5. *Numerical simulation values*

Model parameters	Values	Unit
Rear Length of arc (ar)	9.0	mm
Front Length of arc (af)	3.0	mm
Width of arc (b)	4.5	mm
Depth of arc (d)	4.5	Mm
Convective Transfer Coefficient *(h)*	10	W/m^2K
Emission Coefficient (ε)	0.3	
Arc Efficiency (η)	0.8	

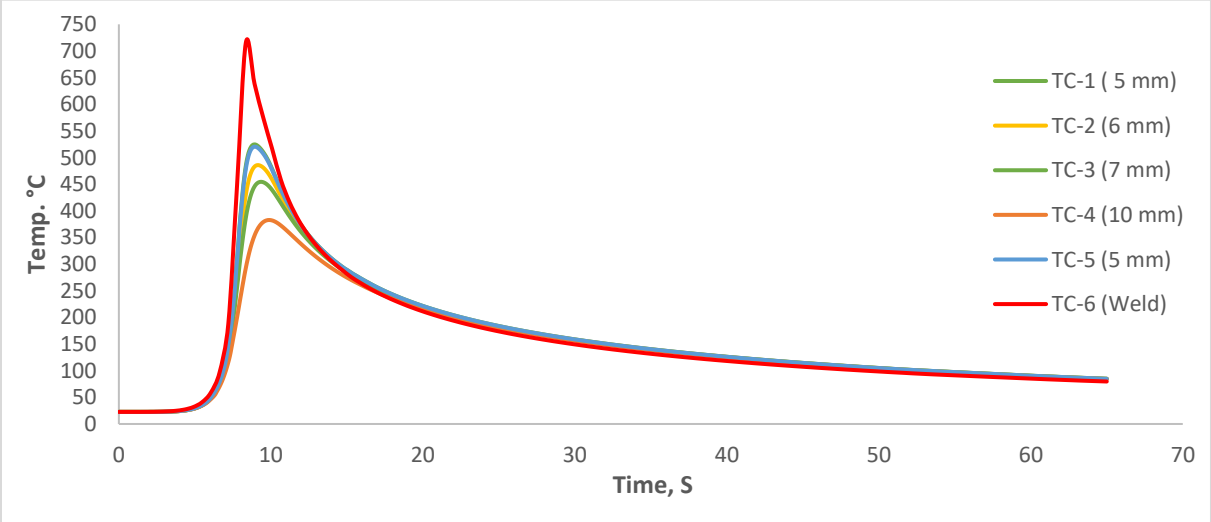

Figure 6. *Numerical simulation of thermal cycle of AW 6005-T6.*

When comparing the numerical and experimental thermal cycles, the trend of the slope of the thermal cycles is similar and the peak temperatures reached are also in an acceptable range. Showing a good agreement between the numerical model and the experimental thermal cycle result.

From the thermal cycles gotten from the welding operation, the peak temperatures above 500 °C for the recrystallization zones that were solutionized aren't sustained for long enough like in the normal T6 treatment, so there may not be enough dissolution of the precipitates for natural hardening in the zone. This brings about a drop in the strength and hardness of the weld joint.

The peak temperature experienced on the plate is a function of the distance from the weld center line where the heat source is placed, this relation can be observed in Figure 6 when the peak temperature is plotted against varying distances from the weld center line. The red points represent the peak temperatures of the thermocouple positions from the welding experiment and the red lines show the positions for each gleeble peak temperature in the weld cross-section. This shows the thermal numerical model represents the welding experiment and the peak temperature experienced on the plate is a function of the distance from the centerline of the weld where the heat source is placed, this relationship can be seen in Figure 7 when the peak temperature is plotted as a function of the different distances from the centerline of the weld. The red dots represent the peak temperatures of the thermocouple positions in the welding experiment and the red lines show the positions for each gleeble peak temperature in the cross-section of the weld. This shows that the thermal numerical model represents the welding experiment and that the gleeble can be located on the weld.

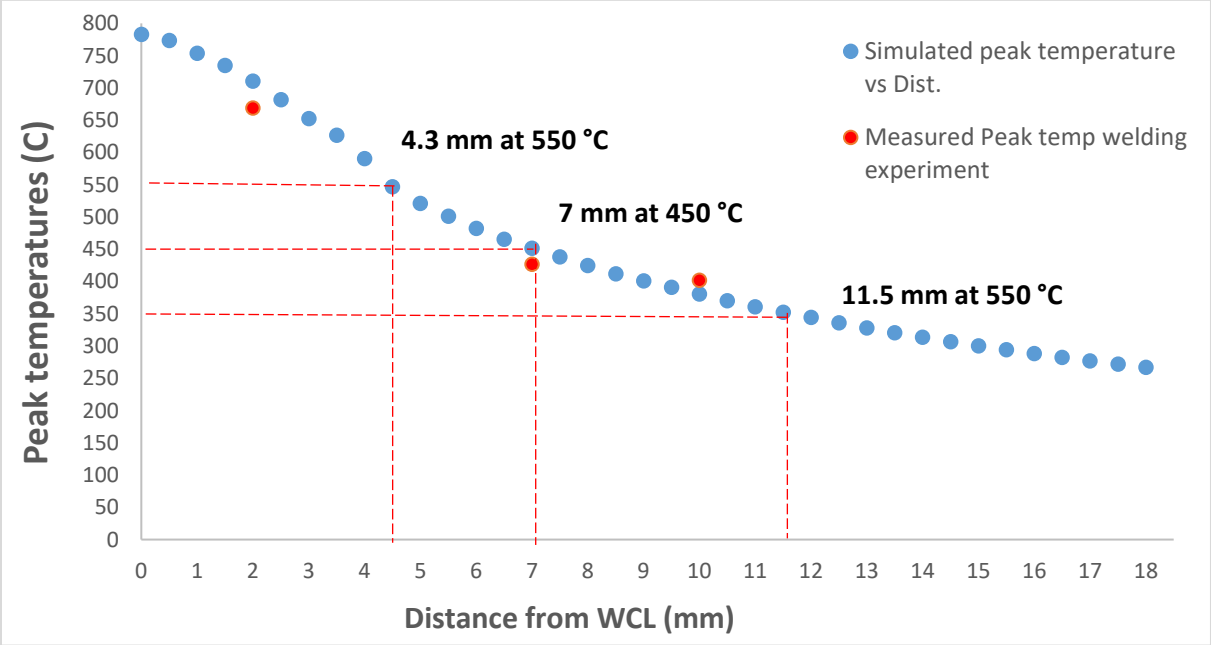

Figure 7. *Peak temperature against distance from WCL.*

Since the temperature in the WCL is 783 °C, this is considerably higher than the melting point of the aluminium alloy which is 655 °C. The welding speed for the operation can be further increased as this will have an economical effect on productivity and decrease the heat input to the alloy. Verification of increasing the welding speed will result in a weld with good fusion in the joint is yet to be seen as further welding experiments weren't carried out for this study.

3.3. Gleeble

Table 6 shows the temperature distribution values of the three samples measured at three different specific locations (0, 7, and 10mm) for each sample during the heat distribution treatment at three different peak temperatures (350 ◦C, 450 ◦C, and 550 ◦C). Figure 8 represents the temperature distribution trendline for the three different peak temperatures (350 ◦C, 450 ◦C, and 550 ◦C).

Table 6. *Peak temperatures sample temperature distribution*

TC	Distance from sample Centre (mm)	550 ºC Specimen	450 ºC Specimen	350 ºC Specimen
TC1	0	550.22	450.52	349.16
TC2	7	523.19	422.25	330.6
TC3	10	467.48	386.25	308.7

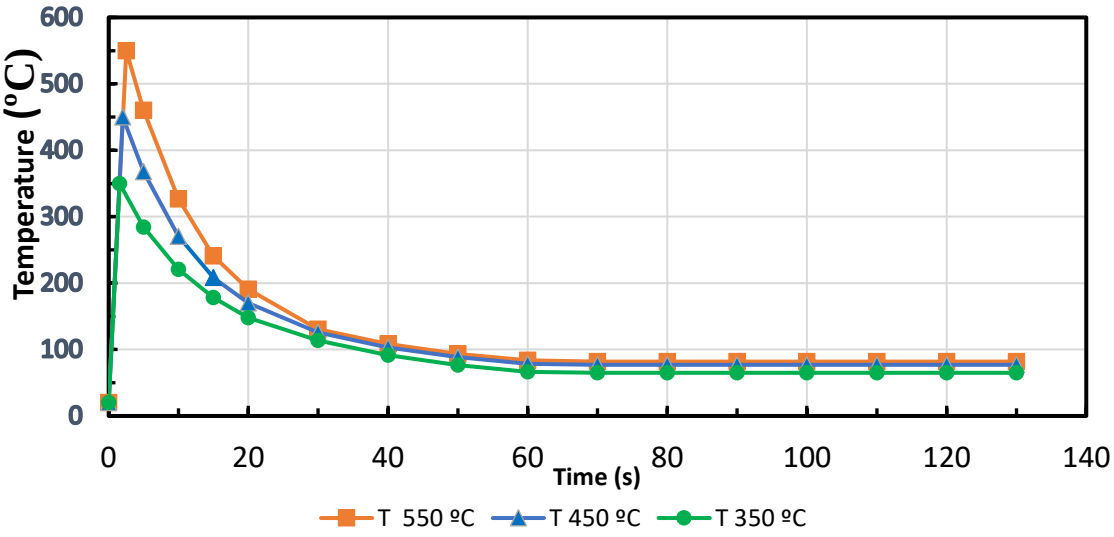

Figure 8. *Temperature distribution curves of the three peak temperatures.*

3.4. Tensile test

The ultimate tensile strength (UTS), the fracture location, and the percentage elongation of the gleeble heat-treated specimens were derived through the tensile test at room temperature. The results are shown in Table 7 and the behaviour of the specimen for the different peak temperatures during the test is shown in Figure 9.

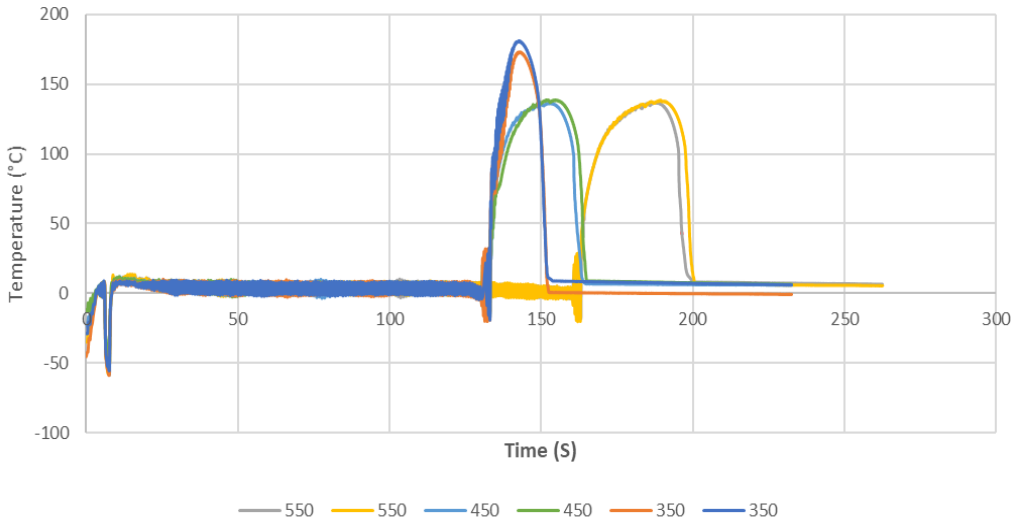

Figure 9. *Tensile results of the peak temperatures.*

Table 7. *Tensile test results for the different peak temperatures.*

Title	Theoretical Peak Temp (°C)	Max Temp (°C)	Max Force (KN)	Max Stress (UTS) (MPa)	Fracture Elongation (%)	Fracture location Estimated mm (from centre)	Temp. At fracture (°C)
350ºC Specimen	350	350.27	5.2	173.13-181.14	10.33	0	350
450ºC Specimen	450	450.2	4.09	136.38-138.75	18.67	7.5	416.73
550ºC Specimen	550	549.5	4.16	136.9 - 138.56	23.67	13.5	335.13

3.5. Metallography results

The metallography was done to examine the microstructures at various parts of the weld microstructure to understand the possible causes for the changes in the mechanical properties of the welded joints. Figure 10 shows the micrograph of the capture for the mounted specimen 1.

A closer look at the specimens can be examined to see the microstructures for some sections of the micrographs. 2 captures were made in the weld cross-section showing the trend of change in the size of the grains in the microstructure.

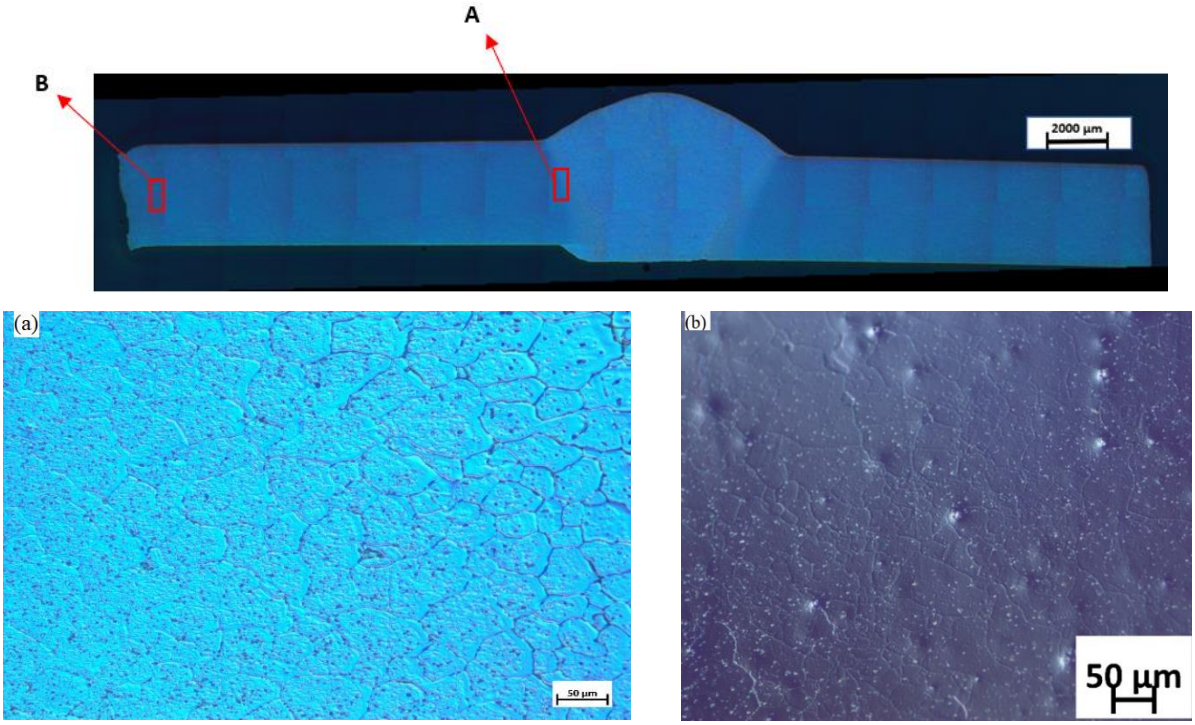

Figure 10. *Micrograph of weld cross-section, a- Zoomed-in HAZ, b)- Zoomed-in BM.*

When comparing figures 10.a and 10.b, it can be observed that the grains in figure 9.a are relatively larger than the grains in 10.b.

3.6. Hardness test results

The linear microhardness results for specimen 1 are given in figure 11 and the microhardness of specimens 2, 3, and 4 are in Table 8.

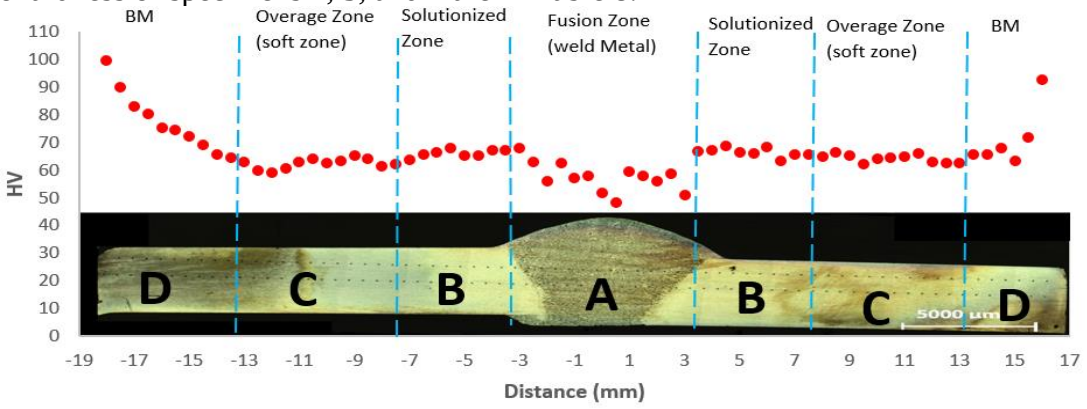

Figure 11. *Vickers hardness profile of the weld cross-section.*

Table 8. *Vickers hardness of specimens*

Sample	HV0.1
Specimen 2 (550 °C Gleeble)	68.1 HV ± 2.0
Specimen 3 (450 °C Gleeble)	62.6 HV ± 1.7
Specimen 4 (350 °C Gleeble)	62.1 HV ± 1.8
Base metal	100.5 HV ± 2.5

Combining the data of peak temperature as a function of distance from the WCL as seen in Figure 7 and the hardness on the weld cross section as a function of the distance from

the WCL, a relationship between the hardness of the cross section as a function of the peak temperature at those points can be obtained as shown in Figure 12.

In the relationship between the microhardness and peak temperature, it can be seen that the minimum microhardness is observed in the fusion zone (FZ) as a result of the filler material used for the welding. The temperature conditions with the least microhardness on the weld are between 330 – 350 °C. Between 270 – 330 °C, there is a gradual increase in the microhardness as it reaches the BM finally, below 270 °C, the microhardness reaches the value for the BM. The red diamonds represent the Gleeble samples hardness values and indicate the hardness lies in the range of the microhardness for the weld cross-section.

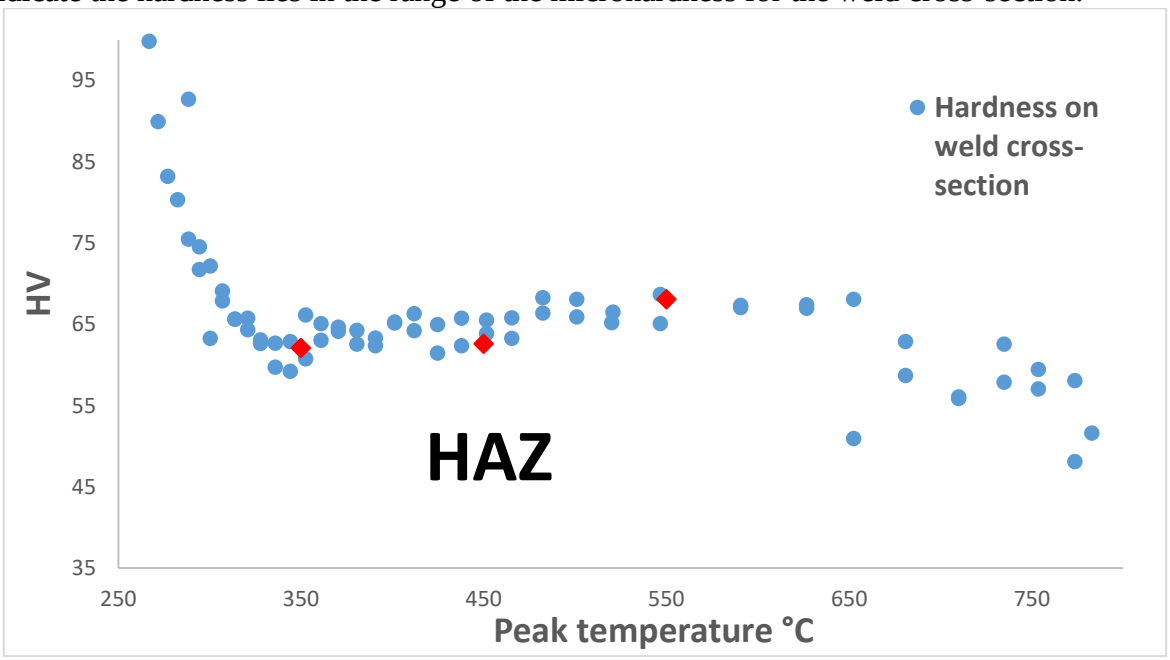

Figure 12. *Hardness against Peak temperature.*

4. Discussion of Results

A comparison between the measurements of the experimental weld and the simulation cross-section as seen in Figure 13 is approximately the same. The height of the weld cross section in the experiment is approximately 5.2 mm and the bead width is 4.0 mm, while for the simulation the height and the width are approximately 5.4 mm and 4.0 mm respectively. This shows the meshed CAD model agrees with the geometry of the real weld cross section.

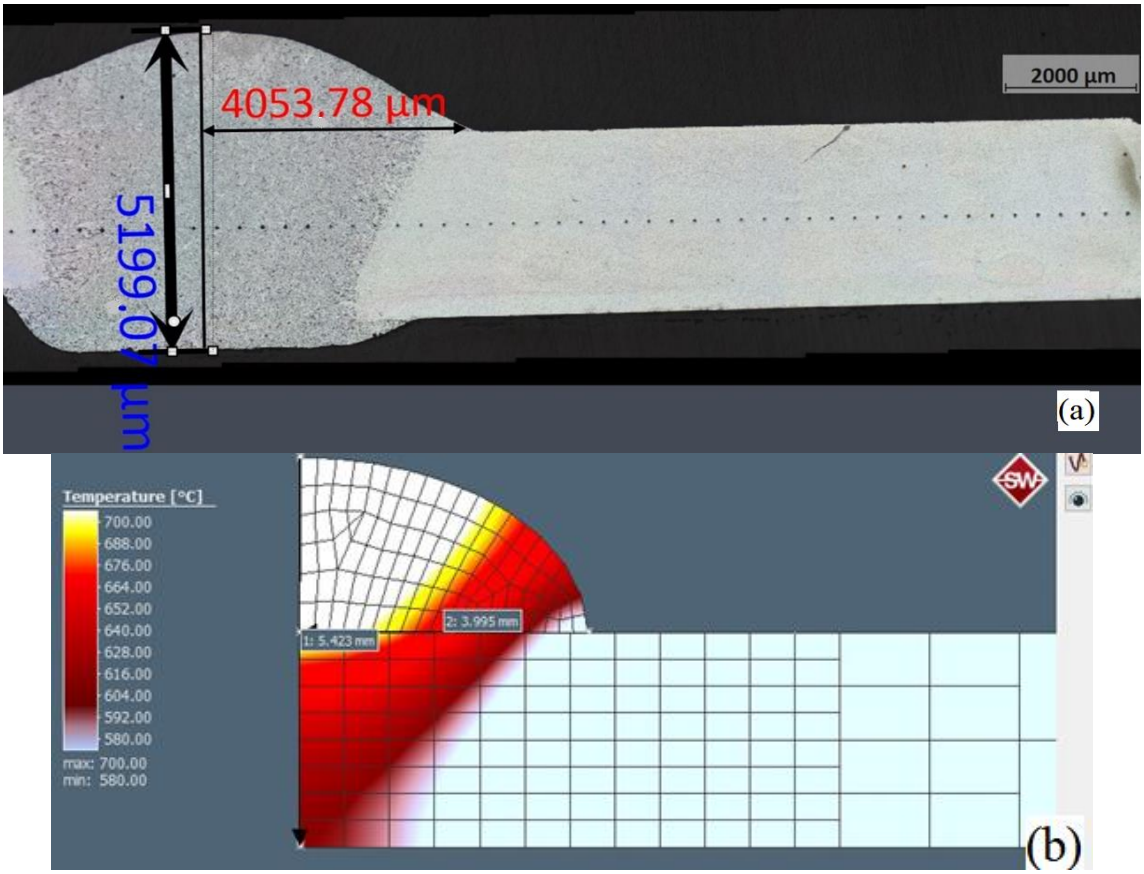

Figure 13. *(a)-Experimental weld-cross section, (b)-Simulation weld-cross section showing the fusion boundary.*

Table 6 shows the Goldak double-ellipsoidal model parameters that were used to simulate the thermal cycle to match the thermal cycle for the welding experiment. The simulated thermal cycles show a good match of the trends of the experimental welding setup, meaning the simulation model is a reasonably accurate representation of the experimental welding operation.

From Table 8 it can be observed that 550 °C specimen has the maximum fracture elongation of 23.67% with the lowest UTS of 138.56 MPa while 350 °C specimen has the lowest fracture elongation of 10.33% and the maximum UTS of 181.14MPa. both having temperatures at fracture as 350 °C and 335.13 °C respectively.

The microhardness profile reported in figure 10 shows agreement with the literature and the FZ, BM, and HAZ for the weld can be identified. The FZ has the lowest microhardness values in the cross section, ranging from 48 HV- 56 HV. The microhardness of the BM is 100 HV, and the HAZ microhardness ranges between 60 HV- 89 HV [18].

In line with the literature, there are slightly higher hardness values close to the fusion line of about 70 HV. This is because the temperature there, over 500 °C is sufficiently high for the precipitates to be dissolved and afterwards possibly, there is natural aging in this region [22; 23; 25; 26]. The drop in hardness in the HAZ may be a result of the temperature being unable to completely solubilize the precipitates, so the precipitates are fewer and grow larger. This occurs in the solution-annealed sub-zone of the HAZ. The microhardness here is about 63.69 HV and a peak temperature treatment is between 350 °C and 500 °C. Farther away from the WCL, there is less heat acting on the alloy, so instead the precipitates don't solubilize but undergo phase transformations and the sizes of the grains in this zone become non-uniform [24; 27; 28]. This sub-zone is called the over-aged zone. It holds the section of the weld with the lowest hardness and may bring about failure upon loading. Other parts in

the over-aged sub-zone with a lower peak temperature acting, experience an increase in mechanical properties before the effect of the heat dissipates from the welded joint. The over-aged zone exists between the peak temperature treatments of 270 °C – 350 °C.

The evidence of these can be seen in the metallography capture of the microstructure with the optical microscope. Figure 9a shows the fusion line, it can be seen that there is a different microstructure in the fusion zone and the HAZ. In figure 10a zoomed-in, it can be noticed that there are some precipitations in the recrystallized zone and the grains in this zone are larger. In figure 9b, the microstructure is composed of grains of varying sizes and what appear to be some precipitations in the matrix. The precipitations in figure 10b farther away from the weld center line are visibly larger with varying sizes. Further confirmation of the phases for the precipitates in the matrix could not be made as this is not possible with the optical microscope.

When comparing the microhardness values of the Gleeble samples from Table 9 to the corresponding microhardness of their positions in the weld cross-section, there is an approximate match. The microhardness values of the selected peak temperatures from both sides of the weld joint in the cross section are shown in Table 9.

Table 9. *Microhardness results at selected peak temperature positions on the weld.*

Peak temperature (°C)	Distance from WCL (mm)	Microhardness (HV0.1)
350	11.5	60 - 63
450	7.0	62 - 66
550	4.3	68 - 70

The HAZ lies approximately between 4 mm to 17.5 mm away from the WCL. Figure 12 shows these regions underwent a peak temperature between 270 °C and 580 °C approximately.

The simulation was also run with values for the heat transfer coefficient on the ceramic backings in the setup, assuming there was heat transfer to the component. It was observed that there was no notable change in the resulting thermal cycles with or without heat transfer to the backings. The amount of heat loss from the plate from equations 7 - 9 depends on the surface area of the component. Comparing the surface areas of the plate and backing, it is evident why the backing's ability to transfer heat has little effect on the resulting thermal condition in the welded plates.

5. Conclusions

This study has investigated the HAZ of AW 6005-T6 butt welded using MIG pulse, numerical simulation was used to further complement the welding experiment results. A clearer understanding of the welding of the alloy can be obtained from the following conclusions: it was possible by proper adjustment of the heat source and boundary condition parameters to model the temperature distribution in the aluminium due to welding. The microhardness of Gleeble samples at 350, 450, and 550 °C are 62, 63, and 68 HV while the weld corresponding to these positions are 62, 64, and 69 HV. The microhardness of the BM is 100 HV, and the mean microhardness in the HAZ is approximately 65 HV. The HAZ of the weld joint lies within 4 mm to 17.5 mm away from the weld centre line. Designing an electric car battery tray using this alloy, it is important to consider the size of the HAZ and the implication of placing another welded joint in its region. This width of HAZ suggests a high heat input from the welding parameters thus a wide area susceptible to failure in the event of loading. The peak temperatures of the heat treatment that was experienced in the weld joint HAZ range between 270 °C – 580 °C. Implying below 270 °C, the thermal cycle is not enough to cause any softening in the alloy. The peak temperature treatment of the over aged

zone in the HAZ lies between 270 °C -330 °C. This indicates the heating conditions at which there is a phase transformation of the precipitates in the alloy. A T6 heat treated aluminium alloy has already been aged to maximum strength, this means further heat input in the HAZ will cause thermal softening in the alloy and lead to a drop in its mechanical properties. It can be observed that the region closes to the fusion line above 500 °C has a higher hardness value. This is a result of the solubilization of the precipitates in the aluminium matrix in that region for natural aging to occur and improve the hardness. Also, it is important to note that a developed numerical simulation model cannot be used to evaluate a welding operation with different welding parameters. Changing the current or travel speed in the model would affect the shape and size of the weld bead, which is input data for the simulation.

The thermocouples placed closest to the fusion line were burnt by the fusion arc and as a result readings from the thermocouples were unusable. An optical microscope isn't adequate for spotting and properly identifying the precipitates and their phases in the aluminium matrix.

The frequency at which the experimental thermal cycle was recorded by the J-thermocouples needs to be increased. So, no potential peak temperature readings may be missed.

The thermocouples placed close to fusion were lost due to the heat from the arc and as a result, a new clamping setup can be developed to allow the thermocouples to be attached to the bottom plates. This way the thermal cycles closer to the WCL can be obtained.

The size of the HAZ from these welding parameters is relatively wide and thus welding parameters with a lower heat input can be developed and investigated. Preferably the welding parameters can be optimized to have a higher welding speed as this will aid industrial productivity and lower the heat input.

Acknowledgement

The authors recognized the support of the Division of Welding Technology, Department of Engineering Science, The Production Technology Centre University West, SE-461 86, Trollhättan, Sweden and Volvo Car Corporation, Göteborg, Sweden.

References

[1] J. Hirsch, « Recent development in aluminium for automotive applications », Transactions of Nonferrous Metals Society of China, vol. 24, no 7, p. 1995-2002, juill. 2014, doi: 10.1016/S1003-6326(14)63305-7.

[2] Verma, R. P., & Lila, M. K. (2021). A short review on aluminium alloys and welding in structural applications. *Materials Today: Proceedings*, *46*, 10687-10691.

[3] Kumagai, M. (2003). Recent technological developments in welding of aluminium and its alloys. *Welding international*, *17*(3), 173-181.

[4] Hirsch, J. (2004). Automotive trends in aluminium-The European perspective. Materials Forum,

[5] Yang, C., Ni, D., Xue, P., Xiao, B., Wang, W., Wang, K., & Ma, Z. (2018). A comparative research on bobbin tool and conventional friction stir welding of Al-Mg-Si alloy plates. *Materials Characterization*, *145*, 20-28.

[6] Sun, T., Franciosa, P., Sokolov, M., & Ceglarek, D. (2020). Challenges and opportunities in laser welding of 6xxx high strength aluminium extrusions in automotive battery tray construction. *Procedia CIRP*, *94*, 565-570.

[7] Famelton, J., Hughes, G., Williams, C., Barbatti, C., Moody, M., & Bagot, P. (2021). Xenon plasma focussed ion beam preparation of an Al-6XXX alloy sample for atom

probe tomography including analysis of an α-Al (Fe, Mn) Si dispersoid. *Materials Characterization*, *178*, 111194.

[8] Dubey, R., Jayaganthan, R., Ruan, D., Gupta, N., Jones, N., & Velmurugan, R. (2022). Energy absorption and dynamic behaviour of 6xxx series aluminium alloys: A review. *International Journal of Impact Engineering*, 104397.

[9] Siwowski, T. W. (2009). Structural behaviour of aluminium bridge deck panels. *Engineering structures*, *31*(7), 1349-1353.

[10] Baharnezhad, S., & Golhin, A. (2017). IN-SITU MEASUREMENT AND FINITE ELEMENT SIMULATION OF THERMO-MECHANICAL PROPERTIES OF AA 6063 ALUMINUM ALLOY FOR MIG WELDMENT. *Materials Physics & Mechanics*, *32*(2).

[11] Goldak, J. A., & Akhlaghi, M. (2005). *Computational welding mechanics*. Springer Science & Business Media.

[12] Wahab, M. A., Painter, M., & Davies, M. (1998). The prediction of the temperature distribution and weld pool geometry in the gas metal arc welding process. *Journal of materials processing technology*, *77*(1-3), 233-239.

[13] Samardžić, I., Stoić, A., Kozak, D., Kladaric, I., & Dunđer, M. (2013). Application of weld thermal cycle simulator in manufacturing engineering. *Manufacturing and Industrial Engineering*, *12*(1-2).

[14] Wu, X., Shuai, J., Xu, K., Lv, Z., & Shan, K. (2020). Determination of local true stress-strain response of X80 and Q235 girth-welded joints based on digital image correlation and numerical simulation. *International Journal of Pressure Vessels and Piping*, *188*, 104232.

[15] Ndiwe, B., Mvola, B., Kah, P., & Bayock, F. N. (2017). Effect of consumable filler wire composition to mismatches of high-Mn steels welded joints. The 27th International Ocean and Polar Engineering Conference,

[16] Nazemi, N., Ghrib, F., & Sokolowski, J. (2013). The HAZ in Aluminum Welding Revisited. 3rd spciality conference on Engineering Mechanics and Materials,

[17] Frappier, R., Benoit, A., Paillard, P., Baudin, T., Le Gall, R., & Dupuy, T. (2014). Quantitative infrared analysis of welding processes: temperature measurement during RSW and CMT-MIG welding. *Science and Technology of Welding and Joining*, *19*(1), 38-43.

[18] Bonazzi, E., Colombini, E., Panari, D., Vergnano, A., Leali, F., & Veronesi, P. (2017). Numerical simulation and experimental validation of MIG welding of T-joints of thin aluminum plates for top class vehicles. *Metallurgical and Materials Transactions A*, *48*, 379-388.

[19] Fernandes, M. F., Torres, M. A. S., Fonseca, M. d. P. C., & Baptista, C. A. R. P. (2020). Investigation of residual stress, stress relaxation and work hardening effects induced by shot peening on the fatigue life of AA 6005-T6 aluminum alloy. *Materials Research Express*, *6*(12), 1265i1262.

[20] Mvola, B., Kah, P., Martikainen, J., & Suoranta, R. (2016). DISSIMILAR HIGH-STRENGTH STEELS: FUSION WELDED JOINTS, MISMATCHES, AND CHALLENGES. *Reviews on Advanced Materials Science*, *44*(2).

[21] Kah, P., Olabode, M., Hiltunen, E., & Martikainen, J. (2013). Welding of a 7025 Al-alloy by a pulsed MIG welding process. *Mechanics*, *19*(1), 96-103.

[22] Spence, C. (2022). Powder Metallurgy Processing of an Al-0.7 Mg-0.4 Si-(Sn) Alloy.

[23] Missori, S., & Sili, A. (2000). Mechanical behaviour of 6082-T6 aluminium alloy welds. *Metallurgical Science and Tecnology*, *18*(1).

[24] Stover, C. M. (1960). Method of Butt Welding Small Thermocouples 0.001 to 0.010 Inch in Diameter. *Review of Scientific Instruments*, *31*(6), 605-608.

[25] « ISO 6892-1:2016(en), Metallic materials — Tensile testing — Part 1: Method of test at room temperature ». https://www.iso.org/obp/ui/#iso:std:iso:6892:-1:ed-2:v1:en (consulté le 23 juillet 2020).
[26] P. NF 94-050, « 94–050. Soils: investigation and testing–determination of moisture content–oven drying method », Association Française de Normalisation, 1995.
[27] ISO standards, "ISO 18273:2015- Welding consumables, wire electrodes, wires and rods for welding of aluminum and aluminum alloys-- classification," iso.org, 2015.
[28] Tsao, C.-S., Chen, C.-Y., Jeng, U.-S., & Kuo, T.-Y. (2006). Precipitation kinetics and transformation of metastable phases in Al–Mg–Si alloys. *Acta Materialia*, *54*(17), 4621-4631.